materials

MDPI

Article

Promoting Effect of Palladium on $ZnAl_2O_4$-Supported Catalysts Based on Cobalt or Copper Oxide on the Activity for the Total Propene Oxidation

Marco Antonio Ocsachoque, María Silvia Leguizamón-Aparicio, Mónica Laura Casella and Ileana Daniela Lick *

CINDECA (CCT La Plata-CONICET-UNLP), Departamento de Química, Facultad de Ciencias Exactas, Universidad Nacional de La Plata, Calle 47 N° 257, La Plata, Buenos Aires 1900, Argentina; ocmarco@quimica.unlp.edu.ar (M.A.O.); mariasilvialap@quimica.unlp.edu.ar (M.S.L.-A.); casella@quimica.unlp.edu.ar (M.L.C.)

* Correspondence: ilick@quimica.unlp.edu.ar; Tel.: +54-221-4211353

Abstract: Palladium-modified Co-ZnAland Cu-ZnAl materials were used and found active for the catalytic oxidation of propene and propane. According to the results obtained by XRD, TPR and XPS, the zinc aluminate-supported phases are oxide phases, Co_3O_4, CuO and PdO_x for Co-ZnAl, Cu-ZnAl and Pd-ZnAl catalysts, respectively. These reducible oxide species present good catalytic activity for the oxidation reactions. The addition of palladium to Co-ZnAl or Cu-ZnAl samples promoted the reducibility of the system and, consequently, produced a synergic effect which enhanced the activity for the propene oxidation. The PdCo-ZnAl sample was the most active and exhibited highly dispersed PdO_x particles and surface structural defects. In addition, it exhibited good catalytic stability. The H_2 pre-treated PdCu-ZnAl, PdCo-ZnAl and Pd-ZnAl samples showed higher activity than the original oxide catalysts, evidencing the important role of the oxidation state of the species, mainly of the palladium species, on the catalytic activity for the propene combustion. The synergic effect between metal transition oxides and PdO_x could not be observed for the propane oxidation.

Keywords: zinc aluminate; palladium; cobalt oxide; copper oxide; propene catalytic oxidation

Citation: Ocsachoque, M.A.; Leguizamón-Aparicio, M.S.; Casella, M.L.; Lick, I.D. Promoting Effect of Palladium on $ZnAl_2O_4$-Supported Catalysts Based on Cobalt or Copper Oxide on the Activity for the Total Propene Oxidation. *Materials* **2021**, *14*, 4814. https://doi.org/10.3390/ma14174814

Academic Editor: Klára Hernádi

Received: 23 July 2021
Accepted: 23 August 2021
Published: 25 August 2021

1. Introduction

Air pollution represents a significant risk to human health. This risk is due to human exposure to toxic pollutants present in the atmosphere, which can cause diseases such as pneumonia, chronic bronchitis and lung cancer. In 2019, the World Health Organization reported that air pollution causes millions of deaths each year [1,2]. Volatile organic compounds (VOCs) are formed of a complex mixture of hundreds of gases that contain carbon, excluding carbon monoxide, carbon dioxide, carbonic acid, metallic carbides or carbonates and ammonium carbonate [3], and can be mentioned among the main atmospheric pollutants. VOCs are generated from several sources, such as industrial processes (e.g., petroleum refining, textile dyeing and printing, etc) and mobile sources (e.g., vehicle engines). Among the compounds called VOCs are saturated alkanes, unsaturated alkenes and alkines, aromatic hydrocarbons, oxygen-containing VOCs and chlorinated VOCs. These compounds can participate in photochemical reactions, in the atmosphere, producing ozone and ultrafine particles that make up photochemical smog [4].The most reactive molecules in this type of photochemical reactions are those that have a C=C double bond in their structure since they allow radicals to be easily added [5]. Therefore, the VOC emission to the atmosphere is an environmental problem that must be solved. In this sense, various processes have been proposed for the elimination of VOCs, such as adsorption on activated carbon, cryogenic condensation, chemical absorption and total catalytic oxidation. The latter being one of the most promising processes [6]. Among the most difficult pollutants to remove by deep catalytic oxidation are the short-chain saturated

and unsaturated hydrocarbons, also called remaining hydrocarbons, which are present in automobile exhaust pipes emissions.

The deep catalytic oxidation, also called combustion, of remaining hydrocarbons has been studied extensively in recent decades. In general, the most used model molecules to study the elimination of short-chain hydrocarbons were those containing low carbon number (<C6) and, particularly, propane and propene (C3). A great variety of catalysts have been reported as active for these oxidations and, to date, numerous works and bibliographic reviews that analyze the state of the art of the subject, have been published [7–25]. These reports include the well know active systems based on the use of supported noble metals (palladium, platinum, ruthenium, gold and rhodium, among others), and systems based on the use of oxide compounds (transition metal oxides, spinels, derivative oxides hydrotalcites, etc.), which, recently, have been studied more extensively.

The noble metal-containing catalysts, and particularly those that contain Pt and Pd, exhibit high activity but present some disadvantages: mainly high cost and low availability [7–9]. Research has focused on minimizing their use or replacing them with oxide catalysts. Although there are numerous bibliographic reports of non-noble metals based catalysts, the bulk transition metal oxides (TMOC) and the supported transition metal oxides catalysts (STMOC) have been found to be very active, mainly those based on the use of Co_3O_4, CuO and MnO_x, among others [11–22,26].

The Co_3O_4, bulk or supported, is considered one of the more promising active oxides, either for the combustion of saturated, unsaturated or polyaromatic hydrocarbons. Its activity in the deep propane oxidation has been widely reported and, also, to a lesser extent, there are reports that show activity for the propene combustion [11–16]. The high activity of this oxide is mainly associated with its redox properties and its lattice oxygen mobility, which can be modified with a suitable choice of the support [17,18]. Another promising active phase is copper oxide, CuO, which has been less studied for this application, but it is known that the addition of CuO to other oxide systems, such as Co_3O_4 or MnO_x increases the activity [19–22,27].

On the other hand, more recent studies focused on the study of the synergy between metallic and non-metallic phases. In some catalytic systems, the addition of small amounts of noble metals (Pt, Pd, Au and Rh) produced an increase in the activity of TMOC and STMOC [28–35]. For example, Kamiuchi et al. reported that the addition of palladium to ceria-zirconia oxide produces an increase in propene combustion [28].In addition, a promotional effect of CeO_2 on palladium supported on alumina pillared clays was found for the deep propene oxidation [36]. Liotta et al. showed that a suitable interaction between supported gold nanoparticles and an oxide support not only improved the catalytic activity of the catalysts for the oxidation of methane, but also improved the catalytic stability [37]. Solsona et al. found that the addition of gold to Co_3O_4–containing catalysts produced an increase in the system reducibility and the oxygen mobility and, consequently, the activity for oxidation reactions is promoted [38]. Similar effects were found in previous works of our working group in which it has been shown that the addition of noble metals (Au, Rh) to cobalt oxide (Co_3O_4) containing catalysts produced an activity increase. For example, the addition of gold to a Co_3O_4/tetragonal zirconia catalyst generated an increase in the activity for the combustion of propane and naphthalene and the addition of rhodium to the Co_3O_4/zinc aluminate system promoted the activity for the deep propane oxidation [29,31].

In addition to the active phase, the nature of the support is another aspect to consider. Generally, the support has an influence on the catalytic activity due to its textural, acid base and redox properties. Although among the most reported supports for these reactions are CeO_2, ZrO_2 and Al_2O_3, however, in recent years has appeared great interest in the use of zinc aluminate, $ZnAl_2O_4$. This oxide has the particularity of presenting great thermal and chemical stability, certain hardness and high specific surface [39,40]. On the other hand, it has been reported that zinc aluminate presents a strong support metal interaction with noble metals, which can favor the stability of the metallic particles [41]. This low-cost support presents the complete spinel structure, which prevents the diffusion

of the supported species in the support network. In a previous work, it has been shown that rhodium-Co_3O_4active phases supported on zinc aluminate exhibited higher activity than a similar alumina-supported catalyst. Zinc aluminate as support leads to a great availability and activity of surface phases [29]. On this basis, this work shows results of cobalt oxide catalysts and copper oxide catalysts supported on non-commercial $ZnAl_2O_4$ for the catalytic combustion of propene, as a model molecule for short-chain unsaturated hydrocarbons. The promoting effect of a small amount of palladium (0.5 wt.%) added to these catalysts is particularly studied. Additionally, the effect of the oxidation state of palladium on activity and some aspects of the reaction mechanism were analyzed. Finally, the prepared catalysts were also tested in the oxidation reaction of propane, a saturated hydrocarbon.

2. Materials and Methods

2.1. Preparation of Support and Catalysts

Zinc aluminate ($ZnAl_2O_4$) was prepared with the coprecipitacion method, from $Zn(NO_3)_2{\cdot}6H_2O$ (Sigma-Aldrich, Argentina) and $Al(NO_3)_3{\cdot}9H_2O$ (Sigma-Aldrich, Argentina) solutions, in ammoniacal medium (pH = 10), following the procedure described elsewhere [29]. This support, labeled ZnAl, was obtained by calcinating at 600 °C. Portions of ZnAl were impregnated with an aqueous solution of Cu or Co nitrates in an ammoniacal medium to obtain materials with 5 wt.% metal concentrations [42]. After being continuously stirred for 6 h, the mixtures were filtered, dried and calcined at 600 °C for 1 h. The monometallic palladium catalyst was prepared by impregnating the zinc aluminate with an aqueous solution of $PdCl_2$ (Sigma-Aldrich, Argentina) to obtain catalysts with a nominal palladium content of 0.5 wt.%. After drying, the sample was calcined under an O_2 flow rate of 60 mL/min at 500 °C for 1 h. Finally, the bimetallic catalysts, containing 0.5 wt.% Pd, were prepared by impregnation of CoO_x and/or CuO_x supported on $ZnAl_2O_4$. Then, the samples obtained were dried and subsequently calcined in O_2 at 500 °C for 1h. The catalysts obtained were labeled as Cu-ZnAl, Co-ZnAl, Pd-ZnAl, PdCu-ZnAl and PdCo-ZnAl.

To study the effect of the palladium oxidation state on the catalytic activity, palladium containing catalysts were thermally treated at 160 °C for 1h in a reducing atmosphere (H_2 10 vol.%/N_2). These samples were labeled as Pd-$ZnAl_{red}$, PdCu-$ZnAl_{red}$ and PdCo-$ZnAl_{red}$.

2.2. Catalyst Characterization

The catalysts were characterized by several physicochemical techniques. The N_2 adsorption–desorption isotherms were obtained using a Micromeritics ASAP 2020 instrument (Micromeritics, Norcross, GA, USA) at −196 °C. Before each measurement, the samples were degassed at 100 °C for 12 h. The specific surface areas were determined by the Brunauer–Emmett-Teller (BET) method.

The crystalline phases were identified by X-ray powder diffraction (XRD) on an X-ray diffractometer (Philips PW 1740, Philips, Eindhoven, The Netherlands) with Cu Kα (Ni-filtered) radiation operated at 20 mA and 40 kV.

In a typical temperature-programmed reduction (H_2-TPR) experiment, the sample (0.1 mg) was placed in an electrically heated fixed-bed quartz micro-reactor, and heated from 25 to 900 °C at a heating rate of 10 °C/min, employing a 10% (v/v) H_2/N_2 (flow rate 20 mL/min) gas mixture.

Scanning electron microscopy with energy-dispersive X-ray spectroscopy (SEM-EDS) analysis was performed in order to obtain elemental mapping and semi-quantitative analyses by using a FEI ESEM Quanta 200 equipment (Thermo Fisher Scientific, formerly FEI Company, Hillsboro, OR, USA).

$$d_{AV} = \frac{\sum n_i d_i^3}{\sum n_i d_i^2} \quad (1)$$

where n_i is the number of particles of d_i size.

Chemical states of cobalt, copper and palladium supported species were investigated by X-ray photoelectron spectroscopy (XPS) on a Physical Electronics PHI-5700 spectrometer, using Al Kα radiation (1486.6 eV). XPS data were calibrated using the binding energy of *C1s* (284.8 eV) as the standard. The Casa XPS program was used for the analysis of the data. Cobalt, copper and palladium spectra were deconvoluted using the least squares fitting routine incorporated in this software with a Gaussian/Lorentzian (30/70) product function, after subtraction of a non-linear baseline. The peak areas obtained were used to determine the surface composition and the sensitivity factors method was applied [43].

2.3. Catalytic Activity

Propene combustion was carried out using an electrically heated fixed-bed quartz reactor containing 0.100 g of catalyst. The catalytic activity was studied with a gaseous mixture feed containing 1000 ppm of C_3H_6, 6 vol.% O_2 and He to close the balance (total flow rate = 50 mL/min).

The catalytic activity for propane oxidation was carried out in a fixed bed quartz reactor containing 0.100 g of catalyst with a feed mixture consisting of C_3H_8/He, O_2/He and He to close the balance. The reaction flow contained 1000 ppm C_3H_8 and 8% v/v O_2. The total gas flow rate was 50 mL/min.

In both processes, the reactant and reaction products streams were analyzed online using a Shimadzu CG 2014 (Shimadzu Corporation, Kyoto, Japan) provided with a TCD. Conversions of C_3H_6 and C_3H_8 to CO_2 were determined from the area of the CO_2 peaks obtained chromatographically. The separation of products was performed with Porapack Q and 5 A molecular sieve columns. The temperature of the catalytic bed was monitored by a k-type thermocouple and the temperature was varied from 150 °C to 600 °C at 1.6 °C/min. A schematic diagram of the reaction systems has been reported in a previous work [44].

The experiments of propene activation were performed in the absence of oxygen, under the same condition adopted for the experiments of propene oxidation by using an on-line mass spectrometer (Dycor, Dymaxion Analyzer, Ametek Process Instruments, Newark, DE, USA) following the most intense molecular ion peaks of C_3H_6 (m/z = 41), CO_2 (m/z = 44) and H_2 (m/z = 2).

3. Results and Discussion

3.1. Characterization of Catalytic Materials

3.1.1. Morphological Characteristics of the Catalysts

Both the support and the catalysts were characterized by N_2 adsorption/desorption, and the experimental data were adjusted by the BET method. All the samples, monometallic and bimetallic catalysts, exhibited type IV isotherms with H1 hysteresis cycle, according to IUPAC. These results indicate that the samples are mesoporous [45]. Figure S1 (Supplementary Material) shows, as an example, the adsorption and desorption isotherms of the support and the PdCo-ZnAl catalyst.

The zinc aluminate support presents a BET area of 50 m^2/g and a pore volume of 0.280 cm^3/g. Cu-ZnAl, Co-ZnAl, Pd-ZnAl and CuPd-ZnAl catalysts show specific surface area and pore volume values such as those observed for the support (Table 1). Instead, the PdCo-ZnAl sample shows a lower specific surface. This fact could be associated with a covering of the pores of the support by new species of cobalt and/or palladium formed during the calcination treatment.

Table 1. BET surface area (S_g), pore volume (V_p) and pore diameter (d_0) of support and catalysts.

Catalyst	V_p (cm^3/g)	S_g (m^2/g)	d_o (nm)
ZnAl	0.280	50	17
Cu-ZnAl	0.274	50	17
Co-ZnAl	0.308	49	16
Pd-ZnAl	0.273	52	15
PdCu-ZnAl	0.276	50	16
PdCo-ZnAl	0.272	42	16

From the desorption isotherm of each sample, the pore diameter (Table 1) was calculated using the BJH method. The results obtained indicate that the addition of the active phases to the support does not lead to a significant modification in the pore diameter of the support.

3.1.2. X-ray Diffraction (XRD)

Powder X-ray diffraction studies were performed to investigate the crystalline phases of both the support and the active species. XRD profiles are presented in Figure 1. All the samples exhibit diffraction lines located at 2θ: 31.29, 36.86, 44.83, 59.39 and 65.27° (PDF 03-065-3104) typical of $ZnAl_2O_4$ [39].

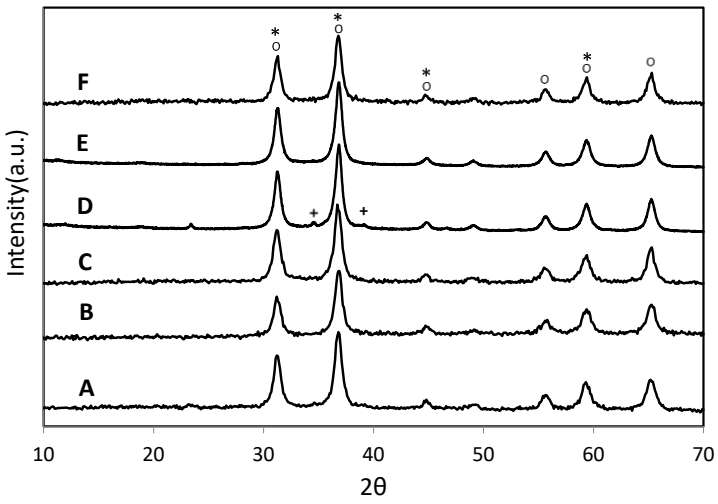

Figure 1. XRD diffractograms of catalysts. (A) ZnAl; (B) Co-ZnAl; (C) Pd-ZnAl; (D) Cu-ZnAl; (E) PdCu-ZnAl and (F) PdCo-ZnAl. ° $ZnAl_2O_4$, * Co_3O_4 and $^+$ CuO.

Neither signals due to ZnO (2θ = 32.01, 34.65, 36.49, 47.77, 56.79, 63.02, 66.59, 68.10 and 69.23°, JCPDS N° 75–1526) were detected, nor signals associated with palladium species, PdO (2θ = 33.60, 33.90, 41.96, 54.84, 60.25 and 60.86°, JCPDS N° 06–0515) nor Pd(0) (2θ = 39.7, 46.5 and 67.9°, JCPDS N° 05–0681). These last diffraction lines cannot be detected because the palladium was added in a very low concentration and the crystallite size of its species is under the resolution of the equipment used.

The diffraction lines of the Co_3O_4 spinel (2θ = 31.2, 36.8, 59.3 and 65.1°, PDF N° 01-080–1533) are difficult to distinguish from those exhibited by the support since both compounds exhibit the same crystalline structure.

The presence of CuO is poorly evidenced in the diffraction profile obtainedfor the Cu-ZnAlsample, withsmall peaks located at 2θ = 35.5 and 38.7° (PDF N° 01-080-1917). However, these signals cannot be evidenced in the XRD pattern of CuPd-ZnAl sample.

3.1.3. Temperature Programmed Reduction (TPR)

To analyze the presence of oxide phases, including those not revealed by XRD, and the palladium addition effect on reducibility, temperature programmed reduction (TPR)

analysis wasperformed. Figure 2 shows the H_2 consumption as a function of temperature for the studied catalysts. In the TPR profile of Pd-ZnAl catalyst (Figure 2, curve C), a low intensity signal at approximately 100 °C can be observed. This signal is assigned to the reduction ofPdO_x [28,46].

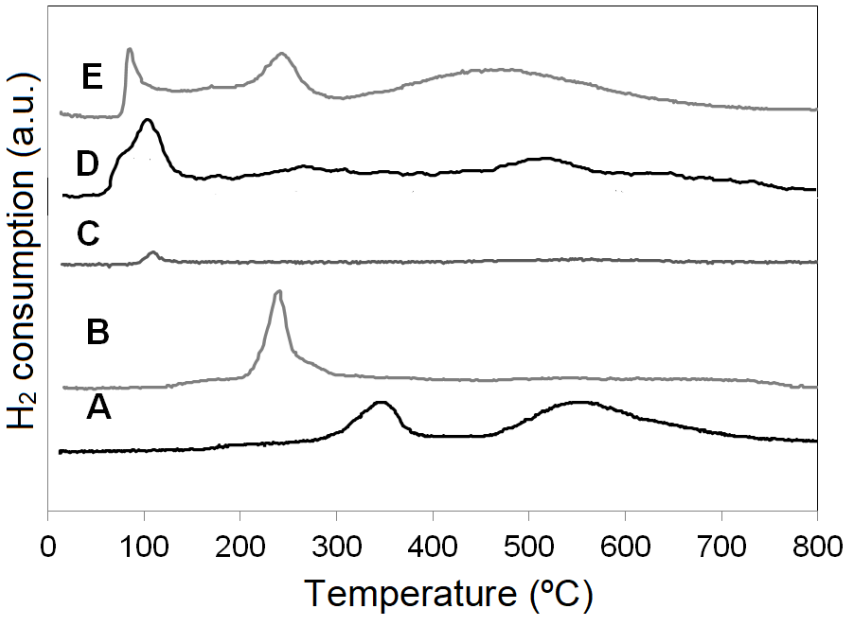

Figure 2. TPR profiles of catalysts. (A) Co-ZnAl; (B) Cu-ZnAl; (C) Pd-ZnAl; (D) PdCu-ZnAl; (E) PdCo-ZnAl.

As it has been reported in a previous work, in the TPR profile of Co-ZnAl catalyst (Figure 2, curve A) two reduction zones can be observed. The first zone, located at temperatures below 400 °C, presents a reduction signal centered around 350 °C and associated with the reduction of Co_3O_4 supported species, weakly interacting with the support. The reduction signal located above 400 °C, centered around 550 °C, is associated with the reduction of cobalt species with a higher interaction with the support [29,47].

The PdCo-ZnAl bimetallic catalyst (Figure 2, curve E) shows H_2 consumption signals starting from 70 °C. The first signal (at ~84 °C) can be associated with the reduction of the oxidized palladium species (PdO_x) and/or the reduction of cobalt oxide species that are in the vicinity and/or in a very close interaction with the palladium oxide. The presence of Pd(0), generated during the reduction, favors the H_2 spillover and, consequently, generates an increase in the reducibility of the rest of the cobalt oxide species and of those cobalt ionic species with greater interaction with the support, which show reduction signals centered at 242 °C and 458 °C, respectively. It is important to note that the reduction signal assigned to the reduction of palladium also shifts towards a lower temperature than that observed for the Pd-ZnAl catalyst, indicating that in this sample the PdO_x species are more dispersed or more available in the catalytic surface.

The Cu-ZnAl catalyst shows (Figure 2, curve B) a reduction signal centered around 240 °C, associated with the reduction of CuO [48], while the PdCu-ZnAl catalyst (Figure 2, curve D) shows a similar behavior to that of the PdCo-ZnAl catalyst. The addition of palladium to Cu-ZnAl catalysts also increases the reducibility of the system. The TPR diagram is dominated by a signal centered at 130 °C, associated with the reduction of dispersed palladium oxide species and CuO. For this system, the reducibility is also favored by the H_2 spillover and, furthermore, it cannot be ruled out that the addition of palladium modified the dispersion or nature of the copper oxide species. Generally, the smaller copper oxide species reduce at a lower temperature. In this context, it should be clarified that, according to the results obtained by XRD, the oxide species present in the PdCu-ZnAl catalyst have smaller crystalline size than those observed in the Cu-ZnAl catalysts. In

addition, at higher temperatures, low intensity signals appear, indicating the presence of some copper species with greater interaction with the support [49,50].

The TPR profiles of palladium containing samples do not present a negative peak around 70 °C, which is associated with the decomposition of the β-PdH phase. This signal is usually observed in TPR profiles of samples that contain palladium metallic species [28]. This fact reinforces the hypothesis of the presence of palladium oxide species.

3.1.4. Scanning Electron Microscopy (SEM) and Energy Dispersive Spectroscopy (EDS)

In order to analyze the morphology and the distribution of the active phases on the catalytic surface, SEM micrographs and EDS elemental mapping were performed. Figure S2Aa–e (Supplementary Material) show SEM images, while Figure S2Ba–j (Supplementary Material) show the Co or Cu, Pd, Al and Zn elemental mapping obtained for each catalyst.

The morphology of catalysts depends on the supported phases, cobalt containing samples (Co-ZnAl or PdCoZnAl) presented larger particles than those found in the Pd-ZnAl sample or copper containing samples (Cu-ZnAl or PdCu-ZnAl).

Elemental mapping images, obtained using magnifications of 300× and 5000×, showed homogeneously dispersed shining points for each element for all the catalysts analyzed. These results suggest that the supported active phases are well distributed and dispersed on the catalytic surface.

SEM-EDS tests were also performed with the purpose of obtaining a semi-quantitative analysis of palladium, copper and cobalt content. The calculated Co/Al, Cu/Al or Pd/Al atomic ratios are listed in Table 2. These atomic ratios obtained are quite higher than the nominal ones, suggesting that the supported oxides are mostly exposed on the catalytic surface.

Table 2. Nominal, EDS-SEM and XPS-derived surface atomic ratios of catalysts.

Catalyst	EDS			XPS			Nominal		
	Co/Al	Cu/Al	Pd/Al	Co/Al	Cu/Al	Pd/Al	Co/Al	Cu/Al	Pd/Al
Co-ZnAl	0.091	-	-	0.22	-	-	0.082	-	-
Cu-ZnAl	-	0.098	-	-	0.083	-	-	0.076	-
Pd-ZnAl	-	-	0.008	-	-	0.004	-	-	0.004
PdCu-ZnAl	-	0.083	0.006	-	0.032	0.005	-	0.076	0.004
PdCo-ZnAl	0.174	-	0.009	0.17	-	0.006	0.082	-	0.004

3.1.5. X-ray Photoelectron Spectroscopy (XPS)

XPS analysis of catalysts was performed to provide information both on the chemical state of the elements and on the surface chemical composition of the studied catalysts.

For the support (Figure S3, Supplementary Material) and all catalysts, the Al 2*p* core level spectrum showed a peak located at 74.4 eV (B.E.) while the Zn 2*p* core level spectrum exhibited a doublet with binding energies at 1022.7 eV and at 1045.8 eV, attributed to the Zn $2p_{3/2}$ and Zn $2p_{1/2}$ components, respectively. The O 1*s* core level spectrum is composed of two components at about 531.6 and at 533.2 eV, attributed to lattice oxygen species, mostly from the support, and adsorbed molecular water, respectively [29]. In agreement with previously reported results for rhodium promoted $Co_3O_4/ZnAl_2O_4$ catalysts, the Al 2*p* Zn 2*p* and O 1*s* core levels spectra are typical of $ZnAl_2O_4$ [29,51].

Palladium-containing catalysts displayed the Pd 3*d* core level spectra with doublets corresponding to Pd $3d_{5/2}$ and Pd $3d_{3/2}$, at 337 and 342 eV, respectively, attributed to Pd(II) species [52–54]. Figure S4 (Supplementary material) shows the Pd 3*d* spectra of catalysts and Table 3 shows the binding energy (B.E.) obtained.

Table 3. XPS Binding energies (B.E.) of palladium, copper and cobalt species, K.E. of cobalt Auger transitions and Co(II)/Co(III) atomic ratios.

	Cu-ZnAl	PdCu-ZnAl	Co-ZnAl	PdCo-ZnAl	Pd-ZnAl
Pd3$d_{5/2}$	-	336.8	-	337.0	336.9
Pd3$d_{3/2}$	-	342.3	-	342.6	342.4
Cu2$p_{3/2}$	933.7	933.5	-	-	-
sat 2$p_{3/2}$	943.1	943.4	-	-	-
Cu2$p_{1/2}$	953.3	953.4	-	-	-
Co 2$p_{3/2}$	-	-	780.9	781.5	
Co 2$p_{1/2}$	-	-	-	-	
sat 2$p_{3/2}$ *	-	-	786.6	786.9	
sat 2$p_{1/2}$ *	-	-	790.1	790.4	
CoLMM Co(III)	-	-	711.7	711.5	
CoLMM Co(II)	-	-	718.3	717.9	
Co(II)/Co(III)	-	-	0.72	0.76	

* Shake-up satellite.

Both cobalt-containing catalysts, Co-ZnAl and PdCo-ZnAl, displayed the Co 2*p* core level spectra with doublets corresponding to Co 2$p_{3/2}$ and Co 2$p_{1/2}$ at ~781 and ~796 eV (Table 3), respectively, separated by spin orbit splitting energy of ~15 eV. Both signals exhibited their respective shake-up satellites. The presence of the satellite corresponding to the Co 2$p_{3/2}$ core level is associated with the presence of Co^{2+} paramagnetic species. Moreover, the Co 2$p_{3/2}$ spectrum is composed of two bands centered at ~780.3 and ~782 eV attributed to Co^{3+} and Co^{2+}, respectively. Figure S5 (Supplementary Material) shows the Co2*p* XPS spectra and the deconvolutions, corresponding to Co-ZnAl and PdCo-ZnAl catalysts. The results obtained suggest the presence of the Co_3O_4 spinel [55–58].

To obtain more precise information about the oxidation states of the cobalt supported species, the CoLMM Auger signals were also analyzed. The chemical shifts of the Auger peaks are generally greater than the photoelectronic ones. Figure 3 shows the spectra in the CoLMM Auger region and Table 3 presents the Co2$p_{3/2}$ peak binding energies (B.E.) and the kinetic energy (KE) of the CoLMM Auger transition. In both samples, modified Auger parameter (AP *) values of ~1549 and 1555 eV were obtained, which are associated with the presence of Co(II) and Co(III) species, respectively [59].

Furthermore, the addition of palladium modifies the chemical environment of cobalt, since the B.E. of these species shifts towards higher values, probably due to the formation of Co-Pd interaction compounds. Likewise, a slight modification of the cobalt oxidation states is also observed, the PdCo-ZnAl catalyst has a higher Co(II)/Co(III) atomic ratio. In this context it is important to note that the values of the Co(II)/Co(III) atomic ratios are higher than the one expected for Co_3O_4-like species for which the atomic ratio is equal to 0.5. These results suggest that the Co^{2+} content originates both from Co_3O_4 spinel structures where the Co(II) ions are tetrahedrally coordinated and from Co(II) ionic species spread on the surface, thereby increasing the Co^{2+}/Co^{3+} ratio. Similar results have been found with rhodium promoted cobalt supported catalysts [29].

The XPS spectra of the Cu2*p* region collected on unpromoted and Pd-promoted catalyst are illustrated in Figure S6 (Supplementary Material). The Cu2*p* core level spectra of Cu-ZnAl and PdCu-ZnAl samples exhibited signals associated with the presence of Cu(II) species on the catalytic surface. In this sense, both catalysts displayed spectra with doublets corresponding to Cu2$p_{3/2}$ andCu 2$p_{1/2}$, at 933.5–933.7 eV and 953.3–953.4 eV [60,61]. These signals exhibit their respective shake-up satellites (Figure S6) that are also associated with the Cu(II) presence [61]. However, the presence of Cu(I) species cannot be completely ruled out, pure CuO exhibits a I_{sat} (intensity of satellite) to a I_{mp} (intensity of the main peak) ratio of 0.55 while the I_{sat}/I_{mp} ratios found for the Cu-ZnAl and PdCu-ZnAl catalysts were below than the theoretical one. On the other hand, the addition of palladium to

the Cu-ZnAl catalyst generates a slight shift of the B.E. of copper towards higher values, evidencing the formation of interaction species [62].

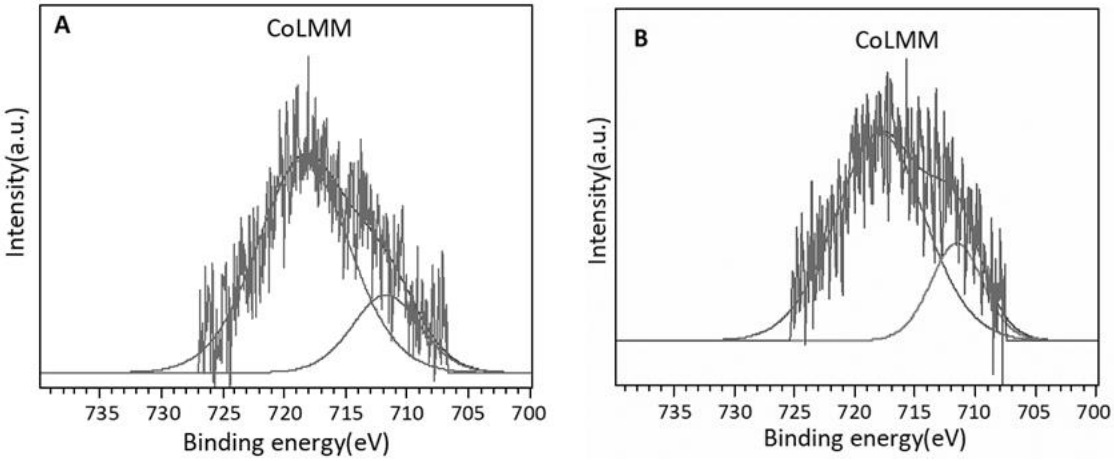

Figure 3. CoLMM Auger region spectra and deconvolutions: (**A**) Co-ZnAl; (**B**) PdCo-ZnAl.

The surface atomic composition was analyzed by integrating the XPS peak areas of the Cu, Co, Pd and Al elements, using the sensitivity factors method [43]. Table 2 summarizes the Co/Al, Cu/Al and Pd/Al surface atomic ratios. The addition of palladium to the Co-ZnAl catalyst causes a decrease in the surface cobalt content. A similar behavior is observed with the addition of palladium to the Cu-ZnAl catalyst. On the other hand, the PdCo-ZnAl and PdCu-ZnAl catalysts have a higher surface Pd content than the Pd-ZnAl catalyst. The sample that exhibits the highest surface concentration of palladium is the PdCo-ZnAl and it exhibits the highest Pd/Al surface atomic ratio. These differences in terms of the surface composition of the catalysts can significantly affect the catalytic behavior of the samples under study.

3.2. Catatytic Activity

3.2.1. Propene Oxidation

The evolution of propene conversion to CO_2 as a function of the reaction temperature is shown in Figure 4, for Co-ZnAl (curve D), Cu-ZnAl (curve E) and Pd-containing catalysts (curves A–C). These experiments were carried out using an O_2/He mixture as oxidizing agent. Table 4 summarizes T_{50} and T_{100} values (temperature at which 50% and 100% conversions are reached, respectively) obtained in each experiment. In the absence of catalyst, propene is poorly oxidized in the O_2/He atmosphere, reaching 10% conversion at 600 °C, while in the presence of the catalysts this hydrocarbon is completely oxidized in the temperature range 150–500 °C, yielding CO_2 as the only observed product (~100% of selectivity).

Table 4. T_{50} and T_{100} obtained with the studied catalysts in propene combustion.

Catalyst	T_{50} (°C)	T_{100} (°C)
Pd-ZnAl	242	384
Cu-ZnAl	305	464
Co-ZnAl	278	377
PdCo-ZnAl	219	331
PdCu-ZnAl	232	340
Pd-ZnAl$_{red}$	197	333
PdCu-ZnAl$_{red}$	203	335
PdCo-ZnAl$_{red}$	191	303

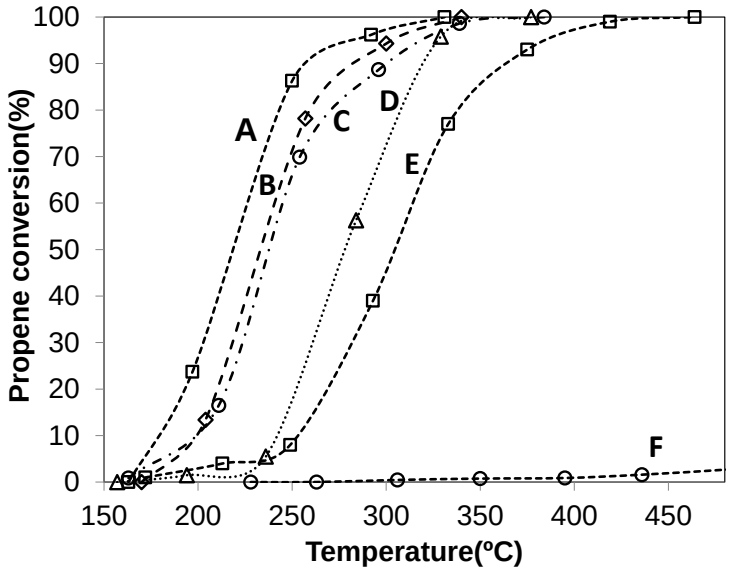

Figure 4. Propene to CO_2 conversion vs. temperature. (A) PdCo-ZnAl; (B) PdCu-ZnAl; (C) Pd-ZnAl; (D) Co-ZnAl; (E) Cu-ZnAl; (F) without catalyst.

Comparing Co-ZnAl and Cu-ZnAl samples, the Co-ZnAl catalyst was the most active and reached a conversion of 50% at 278 °C (T_{50}) (Figure 4, curve D). It is evident that the supported oxide phases, and particularly the cobalt spinel, present the necessary redox properties to promote the oxidation of propene. The Pd-ZnAl catalyst, although it contains a very low concentration of PdO_x, shows very good activity (Figure 4, curve C). The higher activity of this catalyst can be associated with the greater reducibility of the system, since the monometallic catalyst reduces at a lower temperature.

With respect to the effect of Pd content on activity, the palladium-promoted oxide catalysts presented higher activity than the Co-ZnAl and Cu-ZnAl catalysts, as depicted in Figure 4 and in Table 4. The addition of a small amount of palladium (0.5 wt.%) caused a significant increase in the activity. These results suggest that there is a strong synergism between palladium and cobalt or copper species, all oxides contributing as components of the surface-active phase, as it has been reported for other catalytic formulations that contain an oxide phase and precious metals in their composition [28,36]. The synergic effect of Pd-CoO_x or Pd-CuO_x can be evidenced by changes both in the nature of the active sites and in their activity.

For hydrocarbons oxidation reactions, the reducibility of the system, the oxygen mobility and the presence of surface defects are factors that might condition the activity. In this work, the synergic effect could be associated with an increase in the reducibility of the catalytic systems for PdCu-ZnAl and PdCo-ZnAl catalysts, as observed in TPR analysis, and an increase in the surface defects for the cobalt-containing sample, which presented a higher Co(II)/Co(III) surface atomic ratio. Besides, the presence of the Co_3O_4 phase causes an increase in the PdO_x dispersion. TEM micrographs of Pd-ZnAl and PdCo-ZnAl catalysts (Figure S7A) showed particles of PdO_x highly dispersed on both catalysts. The histograms of PdO_x particle size distribution presented in Figure S7B showed that the supported particles had sizes of between 3 and 9 nm for both Pd-ZnAl and PdCo-ZnAl catalysts. The histogram of the PdCo-ZnAl sample exhibited a higher proportion of smaller particles. The average particle diameter (Dva) calculated from the histograms of particle size distribution was 6.0 nm and 5.4 nm for Pd-ZnAl and PdCo-ZnAl, respectively.

The PdCo-ZnAl catalyst (Figure 4, curve A) presented the highest activity and reached the 50% of propane conversion at 219 °C (T_{50}). This sample exhibited some of the characteristics required for oxidation catalysts, high reducibility and surface structural defects. For hydrocarbon oxidation reactions, it was found that the non-ordered or partially ordered cobalt oxide catalysts were more active than the ordered one. In this context, it has been

reported that increasing surface disorder produces an increase in the concentration of reactive oxygen defects and, consequently, an increase in the oxygen mobility [56,63,64]. In addition, the PdO_x particles are more dispersed on the catalytic surface of this catalyst.

It is important to point out that the materials studied in this work, and particularly the PdCo-ZnAl catalyst, presented high activity, comparable to those reported in the literature [8,65–76]. For comparative purposes, a selection of reported catalytic results, in terms of the required temperature to obtain 50% of propene oxidation, is presented in Table 5. It is important to highlight that the catalysts presented in this work contain a low content of noble metal (0.5 wt.%) and show good activity when they are evaluated at an acceptable space velocity (GHSV = 39,500 h^{-1}). For example, in a recent work, Li et al. [8] reported that an alumina-supported Pt nanoparticle (NPs) (2.8 wt.% Pt) catalyst showed a very good performance for the propene combustion, with a T_{50} of 250 °C (GHSV = 30,000 h^{-1}).

Table 5. Comparison of deep propene oxidation activity for different catalysts.

Catalyst	T_{50} (°C)	GHSV (h^{-1})	Reference
PdCo-ZnAl	219	39,500	This work
Co-ZnAl	278	39,500	This work
$Pt(5)Al_2O_3$	210	60,000	[68]
Pd(2)/Al-PILC	210	20,000	[69]
Pt(2)/Al-PILC	310	20,000	[69]
Co/M-Clay	302	50,000	[65]
$Pt(2.8)\gamma$-Al_2O_3	250	30,000	[8]
Pd(1)Al	201	60,000	[67]
Co_3O_4-SSgm	300	45,000	[16]
$Co_{2.1}Fe_{0.9}O_4$	348	45,000	[70]
Pd (0.5)/CeO_2	189	35,000	[6]
$Pd(1.5)TiO_2$	226	60,000	[72]
$Ir(0.5)Au(1)TiO_2$	285	7800	[73]
$Au(1)TiO_2$	242	35,000	[74]
$Au(1)Al_2O_3$	286	35,000	[74]
$Pd(0.5)Au(1)TiO_2$	208	60,000	[72]
$Au(3.07)Ce_{0,3}Ti_{0,7}O_2$	242	60,000	[75]
$Au(3.7)CeO_2$	170	60,000	[76]

3.2.2. Catalytic Stability for the Propene Oxidation

Catalytic stability of PdCo-ZnAl sample was evaluated using two methods. In the first method, the stability was evaluated performing three successive catalytic cycles (Figure 5A), while in the second one, the stability at high conversion values was assessed using an isothermal 24 h experiment, performed at 310 °C (Figure 5B).

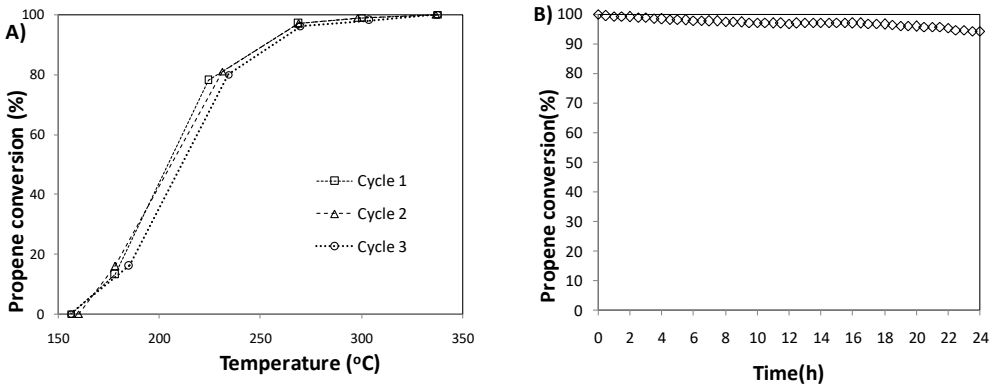

Figure 5. Stability tests for the PdCo-ZnAl catalyst. (**A**) Propane conversion for three successive complete cycles; (**B**) Isothermal stability test at 310 °C for 24 h.

No significant temperature shifts were detected in the conversion curves obtained for the three catalytic cycles. Only a slight shift (~10 °C) of the temperatures that correspond to ~18% and ~80% conversion towards higher values were observed. The stability test performed in an isothermal experiment, at high temperature (310 °C), also revealed that no significant activity loss was observed. While the initial conversion is 100%, after 24 h it decreased to 94%. The results obtained suggest that PdCo-ZnAl catalyst exhibit a very good catalytic stability.

Two mechanisms have been proposed to explain hydrocarbons oxidation reactions, one of them is the redox Mars–van Krevelen mechanism, where the catalytic surface provides active oxygen for the reaction, and the other is a Langmuir–Hinshelwood mechanism, which proposes the existence of active adsorption sites where the reactants, hydrocarbons and oxygen species, interact and are transformed into products [77,78]. To analyze some aspects related to the reaction mechanisms that would allow explaining the differences in the catalytic behavior of the catalysts, complementary experiments were carried out with a feed of propene/helium in the absence of O_2 (g), in a flow reactor *on-line* with a mass spectrometer. These experiments were carried out to analyze if the active phases of catalysts could provide oxygen to oxidize the propene and/or activate it. When experiments are conducted in the absence of molecular oxygen, at increasing temperature CO_2 is formed (Figure 6a) and the occurrence of a surface redox reaction can be postulated. The CO_2 produced can only be generated by propene through its reaction with the lattice oxygen of catalysts, following a redox or Mars–van Krevelen mechanism [29,38]. Moreover, it is shown that the catalysts can activate propene and generate H_2 (g) (Figure 6b). Otherwise, in the absence of a catalyst, neither CO_2 nor H_2 are observed.

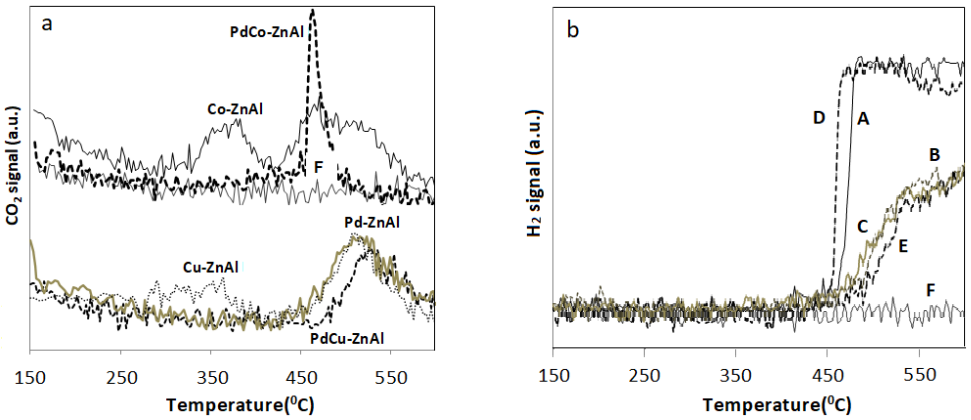

Figure 6. (**a**) CO_2 signal vs. temperature. (**b**) Signal H_2 vs. temperature. (A) Co-ZnAl; (B) Cu-ZnAl; (C) Pd-ZnAl; (D) PdCo-ZnAl; (E) PdCu-ZnAl; (F) without catalyst.

Likewise, the results illustrated in Figure 6 suggest that the temperature range in which propene activation occurs is strongly influenced by the active species present in the catalysts. Co-ZnAl and Cu-ZnAl catalyst start supplying lattice oxygen at ~250 °C and the CO_2 evolution vs. temperature curves showed two maxima, the first at ~350 °C and the second one at ~500 °C, indicating the existence of at least two superficial processes. The first one could be associated with a redox mechanism, while the second one, at higher temperature, could be associated with the propene cracking/activation and H_2 (g) generation, as it is evidenced in Figure 6b. Instead, with palladium-containing catalysts, CO_2 evolution can be observed at higher temperature (>400 °C).

On one hand, it is evident that the formation of Pd-Co or Pd-Cu interaction structures generates a decrease in the availability of lattice oxygen. Moreover, it is evident that the Mars–van-Krevelen mechanism does not completely explain the high activity of the palladium-containing catalysts at low temperature in the presence of O_2 (g), because with these systems the total combustion of propene is reached at a temperature lower than 350 °C. Probably, at low temperature, the reaction mechanism of these catalysts involves the adsorption of both the hydrocarbon and the molecular oxygen, following a Langmuir–Hinshelwood type mechanism.

It is interesting to mention that a TPR profile (not shown) of the post-reaction PdCo-ZnAl sample, used in the presence of molecular oxygen, show lower H_2 consumption at low temperature (<160 °C) than the fresh catalyst. This result suggests that propene could reduce the most accessible active oxide phases during the reaction.

In studies of alkene oxidation reaction mechanisms using metallic catalysts, it has been proposed that the alkene adsorption on the metallic site (e.g., Pt) does not require a previous C–H bond cleavage. The alkene can adsorb via a π bonding between the C=C bond and the metallic atoms. Then, the π-coordinated alkene-metallic species are converted into a di-σ species which leads to C–C bond scission and reaction with adsorbed oxygen [78]. A very strong adsorption of the hydrocarbon could cause a decrease of activity. On the other hand, the importance of the active phase capable of promoting oxygen adsorption should not be discounted and, in this sense, it has been proposed that oxide phases are capable of supplying active oxygen to the metal-oxide interface [6,79]. In this sense, Wan et al. [68] presented a simplified reaction mechanism for the propene oxidation over Pt/BaO/alumina catalysts. In this report, it was proposed that propene adsorbed on the catalytic surface is transformed into carboxilates and formates. Then, these species are oxidized to CO_2 and H_2O. The formation of active oxygen species at the Pt−Ba interface produced an increase in the oxidation rate.

In this context, it is interesting to study the effect of a mild reducing pretreatment (H_2 10% *v/v*, 1 h, 160 °C) on the activity of catalysts. The evolution of the propene conversion with the reaction temperature is shown in Figure 7 and Table 4 summarizes T_{50} and T_{100} values obtained with the pre-treated catalysts.

The H_2 pre-treated samples showed higher activity than the original catalysts, evidencing the important role of the oxidation state of the species, mainly of the palladium species, on the catalytic activity for the propene combustion. Similar results have been reported with zirconia-supported palladium catalysts [28] and with ceria-supported gold catalysts activated with H_2 at 300 °C [80].

The PdCo-ZnAl$_{red}$ sample was the most active (Figure 7, curve B). The T_{50} and T_{100} obtained with this catalyst were 191 and 303 °C, respectively.

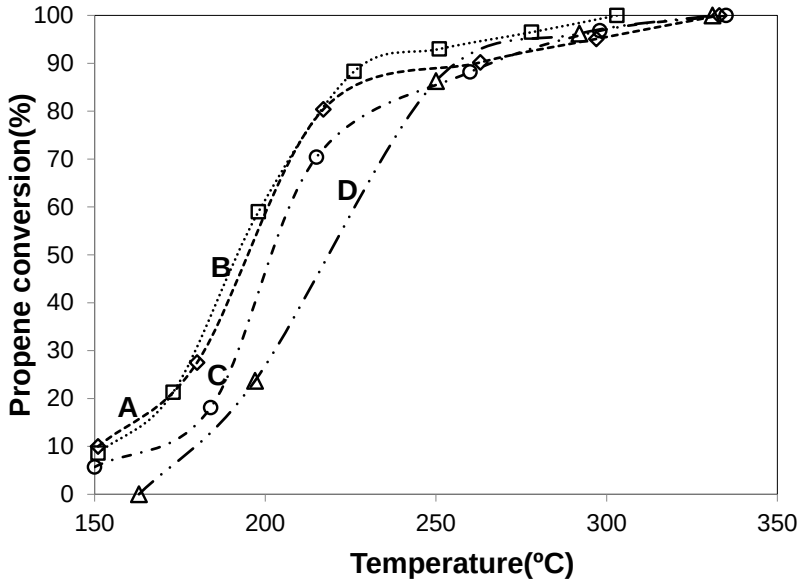

Figure 7. Catalytic activity of H_2 pre-treated catalysts. (A) Pd-ZnAl$_{red}$; (B) PdCo-ZnAl$_{red}$; (C) PdCu-ZnAl$_{red}$; (D) PdCo-ZnAl.

3.2.3. Catalytic Propane Oxidation

In addition to the very good results found in the combustion of propene, catalytic tests were carried out to evaluate the activity of the catalysts for the total oxidation of propane, a model molecule of a saturated short-chain hydrocarbon. The results obtained are shown in Figure 8. In the absence of catalyst, propane is oxidized to CO_2, reaching 50% conversion at 600 °C (T_{50}). Conversely, all the catalysts are active in the temperature range 250–550 °C, reaching the total oxidation of propane yielding CO_2 as the only observed product.

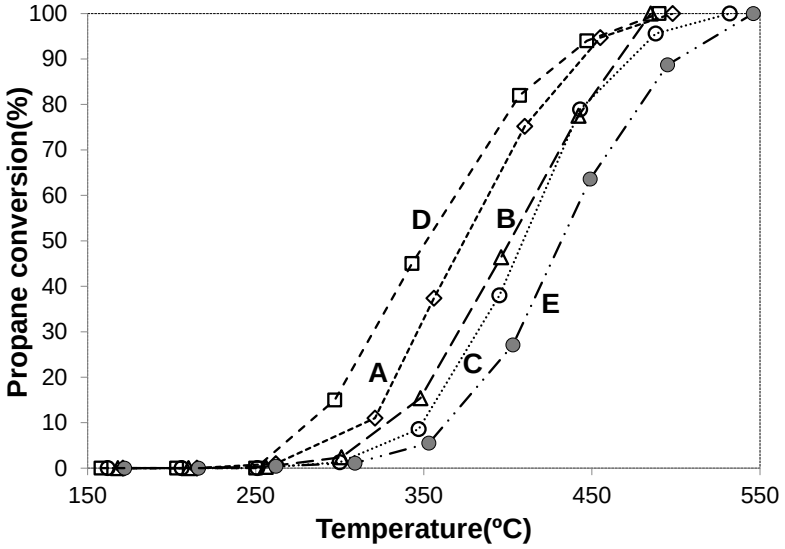

Figure 8. Propane conversion to CO_2 vs. temperature. (A) PdCo-ZnAl; (B) PdCu-ZnAl; (C) Pd-ZnAl; (D) Co-ZnAl; (E) Cu-ZnAl.

For this reaction, the Cu-ZnAl, Pd-ZnAl and PdCu-ZnAl catalysts did not show high activity. Catalysts based on the use of cobalt show higher activity, but for this reaction the addition of palladium does not generate a synergic effect. According to previous reported results [81,82], the palladium-based systems studied in this work did not have high efficiency for propane oxidation. Clearly, this catalyst cannot activate this saturated molecule as effectively as it does with the unsaturated molecule.

4. Conclusions

This paper reported the preparation of PdO_x and/or MO_x $ZnAl_2O_4$-supported catalysts (M = Co, Cu) for the catalytic combustion of propene. The prepared catalysts were examined by using various analytical techniques (BET, XRD, TPR and XPS). It was observed that both transition metals and palladium species are, predominantly, in the form of oxide species. The catalysts were tested for the catalytic combustion of propene and propane. Their activities depended on the nature of the molecule to be oxidized and were influenced by the reducibility of the system. Particularly, the PdCo-ZnAl catalysts exhibited very good performance in the oxidation of propene.

In both the propene and propane combustion reactions, the results obtained showthat Co_3O_4–containingcatalysts supported on $ZnAlO_4$are more active than those containing CuO.

Noble metal addition to Cu-ZnAl and Co-ZnAl catalysts produces a promoting effect on the propene oxidation. These promoted solid presents high activity and their catalytic behavior is associated with a synergistic effect between palladium species and MO_x (M = Co, Cu), which is also evidenced by an increase in the reducibility of the catalytic systems.

Supplementary Materials: The following are available online at https://www.mdpi.com/article/10.3390/ma14174814/s1, Figure S1: Adsorption/desorption isotherms obtained for the ZnAl support (A) and the PdCo-ZnAl catalyst (B), Figure S2A: SEM micrographs of catalysts, Figure S2B: EDS elemental maps, Figure S3: XPS spectra of support, Figure S4: Pd 3d XPS spectra of catalysts. (A) Pd-ZnAl; (B) PdCu-ZnAl; (C) PdCo-ZnAl, Figure S5: Co 2p XPS spectra and deconvolution. (A) Co-ZnAl catalyst; (B) PdCo-ZnAl catalyst, Figure S6: Cu 2p XPS spectra of catalysts. (A) Cu-ZnAl; (B) PdCu-ZnAl, Figure S7A: TEM micrographs of catalysts. (a) ZnAl support; (b) Pd-ZnAl and (c) PdCo-ZnAl, Figure S7B: Histograms of PdOx particle size distribution. (a) Pd-ZnAl and (b) PdCo-ZnAl.

Author Contributions: Conceptualization, I.D.L. and M.A.O.; methodology, I.D.L. and M.A.O.; validation, I.D.L. and M.L.C.; formal analysis, M.S.L.-A. and M.A.O.; investigation, M.S.L.-A., I.D.L. and M.A.O.; resources, I.D.L. and M.L.C.; data curation, M.A.O. and I.D.L.; writing—original draft preparation, M.S.L.-A., M.A.O. and I.D.L.; writing—review and editing, M.L.C. and I.D.L.; visualization, I.D.L.; supervision, I.D.L.; project administration, M.L.C.; funding acquisition, I.D.L. and M.L.C. All authors have read and agreed to the published version of the manuscript.

Funding: This research was funded by Consejo Nacional de Investigaciones Científicas y Técnicas, Agencia Nacional de Promoción Científica y Tecnológica: PICT 0737, Universidad Nacional de La Plata: X903.

Institutional Review Board Statement: Not applicable.

Informed Consent Statement: Not applicable.

Data Availability Statement: Data are contained within the article and can be requested from the corresponding author.

Acknowledgments: The authors acknowledge the financial support of CONICET, ANPCyT and UNLP, and Pablo Fetsis and María Laura Barbelli for characterization experiments.

Conflicts of Interest: The authors declare no conflict of interest.

References

1. World Health Organization. Air Pollution. 2019. Available online: https://www.who.int/airpollution/en/ (accessed on 27 July 2021).
2. Dey, S.; Mehta, N.S. Automobile pollution control using catalysis. *Resour. Environ. Sustain.* **2020**, *2*, 100006. [CrossRef]
3. Technical Overview of Volatile Organic Compounds. Available online: https://www.epa.gov/indoor-air-quality-iaq/technical-overview-volatile-organic-compounds (accessed on 23 July 2021).
4. Li, W.B.; Wang, J.X.; Gong, H. Catalytic combustion of VOCs on non-noble metal catalysts. *Catal. Today* **2009**, *148*, 81–87. [CrossRef]

5. Derwent, R.G.; Jenkin, M.E.; Saunders, S.M.; Pilling, M.J. Photochemical ozone creation potentials for organic compounds in northwest Europe calculated with a master chemical mechanism. *Atmos. Environ.* **1998**, *32*, 2429–2441. [CrossRef]
6. Gil, S.; Garcia-Vargas, J.M.; Liotta, L.F.; Pantaleo, G.; Ousmane, M.; Retailleau, L.; Giroir-Fendler, A. Catalytic Oxidation of Propene over Pd Catalysts Supported on CeO_2, TiO_2, Al_2O_3 and M/Al_2O_3 Oxides (M = Ce, Ti, Fe, Mn). *Catalysts* **2015**, *5*, 671–689. [CrossRef]
7. Liu, G.; Tian, Y.; Zhang, B.; Wang, L.; Zhang, X. Catalytic combustion of VOC on sandwich-structured Pt@ZSM-5 nanosheets prepared by controllable intercalation. *J. Hazard. Mater.* **2019**, *367*, 568–576. [CrossRef] [PubMed]
8. Li, C.; Liu, S.; Yang, F.; Zhang, Y.; Gao, Z.; Yuan, X.; Zheng, X. Synthesis of γ-Al_2O_3–supported Pt nanoparticles using Al-based metal-organic framework as medium and their catalytic performance for total propene oxidation and selective nitrobenzene hydrogenation. *Mater. Chem. Phys.* **2020**, *240*, 122146. [CrossRef]
9. Dong, T.; Liu, W.; Ma, M.; Peng, H.; Yang, S.; Tao, J.; He, C.; Wang, L.; Peng, W.; An, T. Hierarchical zeolite enveloping Pd-CeO_2 nanowires: An efficient adsorption/catalysis bifunctional catalyst for low temperature propane total degradation. *Chem. Eng. J.* **2020**, *393*, 124717. [CrossRef]
10. Yang, X.; Li, Q.; Lu, E.; Wang, Z.; Gong, X.; Yu, Z.; Guo, Y.; Wang, L.; Guo, Y.; Zhan, W.; et al. Taming the stability of Pd active phases through a compartmentalizing strategy toward nanostructured catalyst supports. *Nat. Commun.* **2019**, *10*, 1611. [CrossRef]
11. Liu, Z.; Cheng, L.; Zeng, J.; Hu, X.; Zhangxue, S.; Yuan, S.; Bo, Q.; Zhang, B.; Jiang, Y. Synthesis, characterization and catalytic performance of nanocrystalline Co_3O_4 towards propane combustion: Effects of small molecular carboxylic acids. *J. Solid State Chem.* **2020**, *292*, 121712. [CrossRef]
12. Zhu, Z.Z.; Lu, G.Z.; Zhang, Z.G.; Guo, Y.; Guo, Y.L.; Wang, Y.Q. Highly Active and stable Co_3O_4/ZSM-5 catalyst for propane oxidation: Effect of the preparation method. *ACS Catal.* **2013**, *3*, 1154–1164. [CrossRef]
13. Caia, T.; Deng, W.; Xu, P.; Yuan, J.; Liu, Z.; Zhao, K.; Tong, Q.; He, D. Great activity enhancement of Co_3O_4/γ-Al_2O_3 catalyst for propane combustion by structural modulation. *Chem. Eng. J.* **2020**, *395*, 125071. [CrossRef]
14. Zhang, W.; Wu, F.; Li, J.; You, Z. Dispersion–precipitation synthesis of highly active nanosized Co_3O_4 for catalytic oxidation of carbon monoxide and propane. *Appl. Surf. Sci.* **2017**, *411*, 136–143. [CrossRef]
15. Tian, Z.; Bahlawane, N.; Qi, F.; Kohse-Höinghaus, K. Catalytic oxidation of hydrocarbons over Co_3O_4 catalyst prepared by CVD. *Catal. Commun.* **2009**, *11*, 118–122. [CrossRef]
16. Kouotou, P.M.; Pan, G.F.; Weng, J.J.; Fan, S.B.; Tian, Z.Y. Stainless steel grid mesh-supported CVD made Co_3O_4 thin films for catalytic oxidation of VOCs of olefins type at low temperature. *J. Ind. Eng. Chem.* **2016**, *35*, 253–261. [CrossRef]
17. Liu, Y.; Dai, H.; Deng, J.; Xie, S.; Yang, H.; Tan, W.; Han, W.; Jiang, Y.; Guo, G. Mesoporous Co_3O_4-supported gold nanocatalysts: Highly active for the oxidation of carbon monoxide, benzene, toluene, and o-xylene. *J. Catal.* **2014**, *309*, 408–418. [CrossRef]
18. Xie, S.; Deng, J.; Zang, S.; Yang, H.; Guo, G.; Arandiyan, H.; Dai, H. Au–Pd/3DOM Co_3O_4: Highly active and stable nanocatalysts for toluene oxidation. *J. Catal.* **2015**, *322*, 38–48. [CrossRef]
19. Tian, Z.Y.; Herrenbrück, H.J.; Kouotou, P.M.; Vieker, H.; Beyer, A.; Gölzhäuser, A.; Kohse-Höinghaus, K. Facile synthesis of catalytically active copper oxide from pulsed-spray evaporation CVD. *Surf. Coat. Tech.* **2013**, *230*, 33–38. [CrossRef]
20. Grzelaka, K.; Sobczaka, I.; Yang, C.M.; Ziolek, M. Gold-copper catalysts supported on SBA-15 with long and short channels—Characterization and the use in propene oxidation. *Catal. Today* **2020**, *356*, 155–164. [CrossRef]
21. Labaki, M.; Lamonier, J.F.; Siffert, S.; Zhilinskaya, E.A.; Aboukaıs, A. Influence of the preparation method on the activity and stability of copper–zirconium catalysts for propene deep oxidation reaction. *Colloid Surf. Physicochem. Eng. Asp.* **2003**, *227*, 63–75. [CrossRef]
22. Hosseini, S.A.; Niaei, A.; Salari, D.; Alvarez-Galvan, M.C.; Fierro, J.L.G. Study of correlation between activity and structural properties of Cu-(Cr, Mn and Co)$_2$nano mixed oxides in VOC combustión. *Ceram. Int.* **2014**, *40*, 6157–6163. [CrossRef]
23. He, C.; Cheng, J.; Zhang, X.; Douthwaite, M.; Pattisson, S.; Hao, Z. Recent Advances in the catalytic oxidation of volatile organic Compounds: A Review Based on Pollutant Sorts and Sources. *Chem. Rev.* **2019**, *119*, 4471–4568. [CrossRef]
24. Liotta, L.F. Catalytic oxidation of volatile organic compounds on supported noble metals. *Appl. Catal. B Environ.* **2010**, *100*, 403–412. [CrossRef]
25. Lee, J.E.; Ok, Y.S.; Tsang, D.C.W.; Song, J.H.; Jung, S.C.; Park, Y.K. Recent advances in volatile organic compounds abatement by catalysis and catalytic hybrid processes: A critical review. *Sci. Total Environ.* **2020**, *719*, 137405. [CrossRef]
26. Liotta, L.F.; Ousmane, M.; Di Carlo, G.; Pantaleo, G.; Deganello, G.; Marcì, G.; Retailleau, L.; Giroir-Fendler, A. Total oxidation of propene at low temperature over Co_3O_4–CeO_2 mixed oxides: Role of surface oxygen vacancies and bulk oxygen mobility in the catalytic activity. *Appl. Catal. A Gen.* **2008**, *34*, 781–788. [CrossRef]
27. Zhang, W.; Valverde, J.L.; Giroir-Fendler, A. Cu-Co mixed oxide catalysts for the total oxidation of toluene and propane. *Catal. Today* **2021**, inpress. [CrossRef]
28. Kamiuchi, N.; Haneda, M.; Ozawa, M. Propene oxidation over palladium catalysts supported on zirconium rich ceria–zirconia. *Catal. Today* **2015**, *241*, 100–106. [CrossRef]
29. Leguizamón Aparicio, M.S.; Ocsachoque, M.A.; Rodríguez-Castellón, E.; Gazzoli, D.; Casella, M.L.; Lick, I.D. Promoting effect of rhodium on Co/$ZnAl_2O_4$ catalysts for the catalytic combustion of hydrocarbons. *Catal. Today* **2021**, *372*, 2–10. [CrossRef]
30. Zhao, P.P.; Chen, J.; Yu, H.B.; Cen, B.H.; Wang, W.Y.; Luo, M.F.; Lu, J.Q. Insights into propane combustion over MoO_3 promoted Pt/ZrO_2 catalysts: The generation of Pt-MoO_3 interface and its promotional role on catalytic activity. *J. Catal.* **2020**, *391*, 80–90. [CrossRef]

31. Leguizamón Aparicio, M.S.; Ruiz, M.L.; Ocsachoque, M.A.; Ponzi, M.I.; Rodríguez-Castellón, E.; Lick, I.D. Propane and naphthalene oxidation over gold-Promoted cobalt catalysts supported on zirconia. *Catalysts* **2020**, *10*, 387. [CrossRef]
32. Lakshmanan, P.; Delannoy, L.; Richard, V.; Me'thivier, C.; Potvin, C.; Louis, C. Total oxidation of propene over $Au/xCeO_2$-Al_2O_3 catalysts: Influence of the CeO_2 loading and the activation treatment. *Appl. Catal. B Environ.* **2010**, *96*, 117–125. [CrossRef]
33. Guo, Y.; Wen, M.; Li, G.; An, T. Recent advances in VOC elimination by catalytic oxidation technology onto various nanoparticles catalysts: A critical review. *Appl. Catal. B Environ.* **2021**, *281*, 119447. [CrossRef]
34. Solsona, B.; Garcia, T.; Agouram, S.; Hutchings, G.J.; Taylor, S.H. The Effect of gold addition on the catalytic performance of copper manganese oxide catalysts for the total oxidation of propane. *Appl. Catal. B Environ.* **2011**, *101*, 388–396. [CrossRef]
35. Liotta, L.F.; Di Carlo, G.; Pantaleo, G.; Venezia, A.M.; Deganello, G.; Merlone Borla, E.; Pidria, M.P. Pd/Co_3O_4 catalyst for CH_4 emissions abatement: Study of SO_2 poisoning effect. *Top. Catal.* **2007**, *42*, 425–428. [CrossRef]
36. Aznárez, A.; Korili, S.A.; Gil, A. The promoting effect of cerium on the characteristics and catalytic performance of palladium supported on alumina pillared clays for the combustion of propene. *Appl. Catal. A Gen.* **2014**, *474*, 95–99. [CrossRef]
37. Liotta, L.F.; Di Carlo, G.; Longo, A.; Pantaleo, G.; Venezia, A.M. Support effect on the catalytic performance of Au/Co_3O_4–CeO_2 catalysts for CO and CH_4 oxidation. *Catal. Today* **2008**, *139*, 174–179. [CrossRef]
38. Solsona, B.; Garcia, T.; Hutchings, G.J.; Taylor, S.H.; Makkee, M. TAP reactor study of the deep oxidation of propane using cobalt oxide and gold-containing cobalt oxide catalysts. *Appl. Catal. A Gen.* **2009**, *365*, 222–230. [CrossRef]
39. Walerczyk, W.; Zawadzki, M.; Okal, J. Characterization of the metallic phase in nanocrystalline $ZnAl_2O_4$-supported Pt catalysts. *Appl. Surf. Sci.* **2011**, *257*, 2394–2400. [CrossRef]
40. Mohanty, P.; Mohapatro, S.; Mahapatra, R.; Mishra, D.K. Low cost synthesis route of spinel $ZnAl_2O_4$. *Mater. Today Proc.* **2021**, *35*, 130–132. [CrossRef]
41. Walerczyk, W.; Zawadzki, M. Structural and catalytic properties of $Pt/ZnAl_2O_4$ as catalyst for VOC total oxidation. *Catal. Today* **2011**, *176*, 159–162. [CrossRef]
42. Leguizamón Aparicio, M.S.; Lick, I.D. Total oxidation of propane and naphthalene from emission sources with supported cobalt catalysts. *React. Kinet. Mech. Cat.* **2016**, *119*, 469–479. [CrossRef]
43. Wagner, C.D.; Davis, L.E.; Zeller, M.V.; Taylor, J.A.; Raymond, R.H.; Gale, L.H. Empirical atomic sensitivity factors for quantitative analysis by electron spectroscopy for chemical analysis. *Surf. Interface Anal.* **1981**, *3*, 211–225. [CrossRef]
44. Montaña, M.; Leguizamón Aparicio, M.S.; Ocsachoque, M.A.; Navas, M.B.; Barros, I.; Rodríguez-Castellón, E.; Casella, M.L.; Lick, I.D. Zirconia-supported silver nanoparticles for the catalytic combustion of pollutants originating from mobile sources. *Catalysts* **2019**, *9*, 297. [CrossRef]
45. Thommes, M.; Kaneko, K.; Neimark, A.V.; Olivier, J.P.; Rodriguez-Reinoso, F.; Rouquerol, J.; Sing, K.S.W. Physisorption of gases, with special reference to the evaluation of surface area and pore size distribution (IUPAC Technical Report). *Pure Appl. Chem.* **2015**, *87*, 1051–1069. [CrossRef]
46. Takeguchi, T.; Okanishi, T.; Aoyama, S.; Ueda, J.; Kikuchi, R.; Eguchi, K. Strong chemical interaction between PdO and $SnO_2$and the influence on catalytic combustion of methane. *Appl. Catal. A Gen.* **2003**, *252*, 205–214. [CrossRef]
47. Martínez, A.; López, C.; Márquez, F.; Díaz, I. Fischer–Tropsch synthesis of hydrocarbons over mesoporous Co/SBA-15 catalysts: The influence of metal loading, cobalt precursor, and promoters. *J. Catal.* **2003**, *220*, 486–499. [CrossRef]
48. Sato, S.; Iijima, M.; Nakayama, T.; Sodesawa, T.; Nozaki, F. Vapor-Phase Dehydrocoupling of Methanol to Methyl Formate over $CuAl_2O_4$. *J. Catal.* **1997**, *169*, 447–454. [CrossRef]
49. Baeza, P.; Aguila, G.; Vargas, G.; Ojeda, J.; Araya, P. Adsorption of thiophene and dibenzothiophene on highly dispersed Cu/ZrO_2 adsorbents. *Appl. Catal. B Environ.* **2012**, *111–112*, 133–140. [CrossRef]
50. Vargas, D.; Rubio, J.M.; Santamaría, J.; Moreno, R.; Mérida, J.M.; Perez, M.A.; Jimenez, A.; Hernandez, R.; Maireles, P. Furfuryl alcohol from furfural hydrogenation over copper supported on SBA-15 silica catalysts. *J. Mol. Catal. A Chem.* **2014**, *383–384*, 106–113. [CrossRef]
51. Strohmeier, B.R. Zinc Aluminate ($ZnAl_2O_4$) by XPS. *Surf. Sci. Spectra* **1994**, *3*, 128–134. [CrossRef]
52. Brun, M.; Berthet, A.; Bertolini, J.C. XPS, AES and Auger parameter of Pd and PdO. *J. Elect. Spec. Rel. Phen.* **1999**, *104*, 55–60. [CrossRef]
53. Briggs, D.; Seah, M.P. *Practical Surface Analysis*, 2nd ed.; Auger and X- Spectroscopy; John Wiley and Sons: Chischester, UK, 1990; Volume 1.
54. Haack, L.P.; Otto, K. X-ray photoelectron spectroscopy of Pd/γ-alumina and Pd foil after catalytic methane oxidation. *Catal. Lett.* **1995**, *34*, 31–40. [CrossRef]
55. Ren, Z.; Wu, Z.; Song, W.; Xiao, W.; Guo, Y.; Ding, J.; Suib, S.L.; Gao, P. Low temperature propane oxidation over Co_3O_4 based nano-array catalysts: Ni dopant effect, reaction mechanism and structural stability. *Appl. Catal. B Environ.* **2016**, *180*, 150–160. [CrossRef]
56. Garcia, T.; Agouram, S.; Sánchez-Royo, J.F.; Murillo, R.; Mastral, A.M.; Aranda, A.; Vázquez, I.; Dejoz, A.; Solsona, B. Deep oxidation of volatile organic compounds using ordered cobalt oxides prepared by a nanocasting route. *Appl. Catal. A Gen.* **2010**, *386*, 16–27. [CrossRef]
57. Vaz, C.A.F.; Prabhakaran, D.; Altman, E.I.; Henrich, V.E. Experimental study of the interfacial cobalt oxide in Co_3O_4/α–$Al_2O_3(0001)$ epitaxial films. *Phys. Rev. B* **2009**, *80*, 155457. [CrossRef]

58. Petitto, S.C.; Marsh, E.M.; Carson, G.A.; Langell, M.A. Cobalt oxide surface chemistry: The interaction of CoO(1 0 0), Co_3O_4(1 1 0) and Co_3O_4(1 1 1) with oxygen and water. *J. Mol. Catal. A Chem.* **2008**, *281*, 49–58. [CrossRef]
59. Infantes-Molina, A.; Mérida-Robles, J.; Rodríguez-Castellón, E.; Pawelec, B.; Fierro, J.L.G.; Jiménez-López, A. Catalysts basedon Co/zirconium doped mesoporous silica MSU for the hydrogenation and hydrogenolysis/hydrocracking of tetralin. *Appl. Catal. A Gen.* **2005**, *286*, 239–248. [CrossRef]
60. Biesinger, M.C.; Lau, L.W.M.; Gerson, A.R.; Smart, R.S.C. Resolving surface chemical states in XPS analysis of first row transition metals, oxides and hydroxides: Sc, Ti, V, Cu and Zn. *Appl. Surf. Sci.* **2010**, *257*, 887–898. [CrossRef]
61. Poulston, S.; Parlett, P.M.; Stone, P.; Bowker, M. Surface oxidation and reduction of CuO and Cu_2O studied using XPS and XAES. *Surf. Interface Anal.* **1996**, *24*, 811–820. [CrossRef]
62. Bennici, S.; Gervasini, A.; Ravasio, N.; Zaccheria, F. Optimization of tailoring of CuO_x species of silica alumina supported catalysts for the selective catalytic reduction of NO_x. *J. Phys. Chem. B* **2003**, *107*, 5168–5176. [CrossRef]
63. Tang, W.; Xiao, W.; Wang, S.; Ren, Z.; Ding, J.; Gao, P.X. Boosting catalytic propane oxidation over PGM-free Co_3O_4 nanocrystal aggregates through chemical leaching: A comparative study with Pt and Pd based catalysts. *Appl. Catal. B Environ.* **2018**, *226*, 585–595. [CrossRef]
64. Machida, M.; Minami, S.; Hinokuma, S.; Yoshida, H.; Nagao, Y.; Sato, T.; Nakahara, Y. Unusual redox behavior of Rh/$AlPO_4$ and its impact on three-way catalysis. *J. Phys. Chem. C* **2015**, *119*, 373–380. [CrossRef]
65. Assebban, M.; Tian, Z.Y.; El Kasmi, A.; Bahlawane, N.; Harti, S.; Chafik, T. Catalytic complete oxidation of acetylene and propene over clay versus cordierite honeycomb monoliths without and with chemical vapor deposited cobalt oxide. *Chem. Eng. J.* **2015**, *262*, 1252–1259. [CrossRef]
66. Serhal, C.A.; Mallard, I.; Poupin, C.; Labaki, M.; Siffert, S.; Cousin, R. Ultra quick synthesis of hydrotalcite-like compounds as efficient catalysts for the oxidation of volatile organic compounds. *Comptes Rendus Chim.* **2018**, *21*, 993–1000. [CrossRef]
67. Sihaib, Z.; Puleo, F.; Pantaleo, G.; La Parola, V.; Valverde, J.L.; Gil, S.; Liotta, L.F.; Giroir-Fendler, A. The Effect of Citric Acid Concentration on the Properties of $LaMnO_3$ as a Catalyst for Hydrocarbon Oxidation. *Catalysts* **2019**, *9*, 226. [CrossRef]
68. Wan, J.; Ran, R.; Li, M.; Wu, X.D.; Weng, D. Effect of acid and base modification on the catalytic activity of Pt/Al_2O_3 for propene oxidation. *J. Mol. Catal. A Chem.* **2014**, *383*, 194–202. [CrossRef]
69. Aznarez, A.; Gil, A.; Korili, S.A. Performance of palladium and platinum supported on alumina pillared clays in the catalytic combustion of propene. *RSC Adv.* **2015**, *5*, 82296–82309. [CrossRef]
70. Tian, Z.Y.; Kouotou, P.M.; Kasmi, A.E.; Ngamou, P.H.T.; Kohse-Hoinghaus, K.; Vieker, H.; Beyer, A.; Golzhauser, A. Low-temperature deep oxidation of olefins and DME over cobalt ferrite. *Proc. Combust. Inst.* **2015**, *35*, 2207–2214. [CrossRef]
71. Iwanek, E.M.; Liotta, L.F.; Williams, S.; Hu, L.; Clailung, K.; Pantaleo, G.; Kaskur, Z.; Kirk, D.W.; Gliński, M. Application of potassium ion deposition in determining the impact of support reducibility on catalytic activity of Au/ceria-zirconia catalysts in CO oxidation, NO oxidation, and C_3H_8 combustion. *Catalysts* **2020**, *10*, 688. [CrossRef]
72. Hosseini, M.; Siffert, S.; Tidahy, H.L.; Cousin, R.; Lamonier, J.F.; Aboukais, A.; Vantomme, A.; Roussel, M.; Su, B.L. Promotional effect of gold added to palladium supported on a new mesoporous TiO_2 for total oxidation of volatile organic compounds. *Catal. Today* **2007**, *122*, 391–396. [CrossRef]
73. Aguilar-Tapia, A.; Zanella, R.; Calers, C.; Louis, C.; Delannoy, L. Synergetic Effect in bimetallic Ir-Au/TiO_2 catalysts in the total oxidation propene: Influence of the activation conditions. *Phys. Chem. Chem. Phys.* **2015**, *17*, 28022–28032. [CrossRef] [PubMed]
74. Ousmane, M.; Liotta, L.F.; Pantaleo, G.; Venezia, A.M.; Di Carlo, G.; Aouine, M.; Retailleau, L.; Giroir-Fendler, A. Supported Au catalysts for propene total oxidation: Study of support morphology and gold particle size effects. *Catal. Today* **2011**, *176*, 7–13. [CrossRef]
75. Lamallem, M.; Cousin, R.; Thomas, R.; Siffert, S.; Aïssi, F.; Aboukaïs, A. Investigation of the effect of support thermal treatment on gold-based catalysts activity towards propene total oxidation. *Comptes Rendus Chim.* **2009**, *12*, 772–778. [CrossRef]
76. Aboukaïs, A.; Skaf, M.; Hany, S.; Cousin, R.; Aouad, S.; Labaki, M.; Abi-Aad, E. A Comparative study of Cu, Ag and Au doped CeO_2 in the total oxidation of volatile organic compounds (VOCs). *Mater. Chem. Phys.* **2016**, *177*, 570–576. [CrossRef]
77. Yao, Y.F.Y. The oxidation of CO and hydrocarbons over noble metal catalysts. *J. Catal.* **1984**, *87*, 152–162. [CrossRef]
78. Diehl, F.; Barbier, J.; Duprez, D.; Guibard, I.; Mabilon, G. Catalytic oxidation of heavy hydrocarbons over Pt/Al_2O_3. Influence of the structure of the molecule on its reactivity. *Appl. Catal. B Environ.* **2010**, *95*, 217–227. [CrossRef]
79. Zhou, Z.; Harold, M.P.; Luss, D. Enhanced NO, CO and C_3H_6 conversion on Pt/Pd catalysts: Impact of oxygen storage material and catalyst architecture. *Catal. Today* **2021**, *360*, 375–387. [CrossRef]
80. Delannoy, L.; Fajerwerg, K.; Lakshmanan, P.; Potvin, C.; Methivier, C.; Louis, C. Supported gold catalysts for the decomposition of VOC: Total oxidation of propene in low concentration as model reaction. *Appl. Catal. B Environ.* **2010**, *94*, 117–124. [CrossRef]
81. Bae, J.; Kim, J.; Jeong, H.; Lee, H. CO oxidation on SnO_2 surfaces enhanced by metal doping. *Catal. Sci. Technol.* **2018**, *8*, 782–789. [CrossRef]
82. Solsona, B.; Sanchis, R.; Dejoz, A.M.; García, T.; Ruiz-Rodríguez, L.; López Nieto, J.M.; Cecilia, J.A.; Rodríguez-Castellón, E. Total oxidation of propane using CeO_2 and CuO-CeO_2 catalysts prepared using templates of different nature. *Catalysts* **2017**, *7*, 96. [CrossRef]